

## DUAL-BAND DIFFERENTIAL FILTER USING BROAD-BAND COMMON-MODE REJECTION ARTIFICIAL TRANSMISSION LINE

Armando Fernández-Prieto<sup>1</sup>, Jesús Martel<sup>1</sup>,  
Francisco Medina<sup>1</sup>,\*, Francisco Mesa<sup>1</sup>, Shilong Qian<sup>2</sup>,  
Jia-Sheng Hong<sup>2</sup>, Jordi Naqui<sup>3</sup>, and Ferran Martín<sup>3</sup>

<sup>1</sup>Microwaves Group, Department of Electronics and Electromagnetism and Department of Applied Physics 1 and 2, University of Seville, Av. Reina Mercedes s/n, 41012 Seville, Spain

<sup>2</sup>Department of Electrical, Electronic and Computer Engineering, Heriot-Watt University, Edinburgh, UK

<sup>3</sup>GEMMA/CIMITEC, Departament d'Enginyeria Electrònica, Universitat Autònoma de Barcelona, Spain

**Abstract**—A new balanced dual-band bandpass filter with strong common-mode rejection is presented in this paper. Common-mode rejection is provided by a section of a periodic microstrip differential line that behaves as a low-pass filter under common-mode operation. In contrast, the differential line exhibits very good all-pass behavior under differential mode operation. This structure is combined with a differential dual-band bandpass filter based on embedded resonators. Simulations and experiments confirm that the combined structure has good common-mode rejection within the passbands of the dual-band differential filter.

### 1. INTRODUCTION

Differential signaling plays an essential role in the design of modern high-speed digital circuits because of its comparatively high degree of immunity to noise coming from electromagnetic interference (EMI) and crosstalk. Ideally, differential signal transmission methods meet the tight requirements of EMI compliance and signal integrity but, in practice, any differential signal has some level of common-mode

---

*Received 14 April 2013, Accepted 10 May 2013, Scheduled 21 May 2013*

\* Corresponding author: Francisco Medina (medina@us.es).

noise (mainly caused by amplitude unbalance and time skew). Since this common-mode level can lead to undesired radiation and EMI problems that degrades the performance of high-speed circuitry, a lot of effort has been devoted to the design of differential devices with high common-mode rejection [1–8]. A different approach to achieve good performance is to combine artificial transmission lines providing good common-mode suppression (while keeping the integrity of the differential path) with differential devices (such as bandpass filters) whose common-mode response might not be satisfactory. In the MHz domain, common-mode chokes have traditionally been used to suppress common-mode propagation [9, 10], although such strategy does not work in the GHz domain. In this domain, it was proposed in [11] the use of a LTCC compact narrow band common-mode rejection filter based on coupled lumped inductors. However, the method in [11] makes use of a laborious fabrication process that involves a complicated multilayer structure with via-holes. Alternatively, simpler structures based on etched defected ground structures (DGS) can be used to suppress the common-mode signal. Dumbbell [12] and UH-shaped [13] DGSs have been periodically etched in the ground plane, below a pair of coupled strips signal line, to reject the common-mode noise. Those DGSs can be seen as parallel  $LC$  resonators for the common-mode signals and ideal shorts for the differential signals. Since the common-mode current is forced to flow through the ground plane, the etched defect has a significant influence on that mode whereas the differential mode is slightly affected. Nevertheless, the introduction of slots in the ground plane modifies the differential-mode impedance, leading to some level of mismatch losses for the differential signals. Another metamaterial-inspired solution has recently been demonstrated in [14]. This proposal makes use of complementary split-ring resonators in the ground plane to yield very strong common-mode rejection over a relatively narrow band with no perturbation of the differential mode.

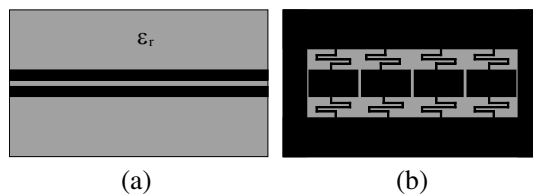


**Figure 1.** Top (a) and bottom (b) metallization patterns corresponding to the common-mode suppression structure analyzed in this paper. Four cells are shown. Black areas correspond to metallized regions.

In this paper, the broadband common-mode filtering transmission structure for GHz differential signals introduced in [15] is studied in depth and used to build a compact high-performance balanced dual-band filter. Dual-band [16–22] and multiband [23–25] components are becoming more and more important in modern wireless systems. Therefore, the implementation of the differential versions of such filters is of great importance [26]. A sketch of the common-mode rejection structure studied in this paper is depicted in Fig. 1 (top and bottom side views). A pair of coupled microstrip lines is loaded with a periodic distribution of centered conductor patches. The patches are symmetrically series connected to the ground plane by means of narrow (high impedance) strip lines. These lines behave as inductors in the frequency range of interest. Under common-mode operation, the pattern printed in the ground plane in conjunction with the coupled lines of the top side behave as a low-pass filter. Common-mode signal is then expected to be strongly rejected over a wide frequency band above a certain adjustable frequency. Simultaneously, the mismatch of the differential line caused by the presence of the slotted ground plane is minimized by properly tuning the dimensions of lines and patches at both sides of the substrate. Thanks to the broadband behavior of that structure, its combination with a simple balanced dual-band filter (with intrinsic poor common-mode rejection) will allow us to implement a balanced dual-band differential filter with good common-mode performance. The dual-band geometry used in this paper is inspired in the single-ended design in [27].

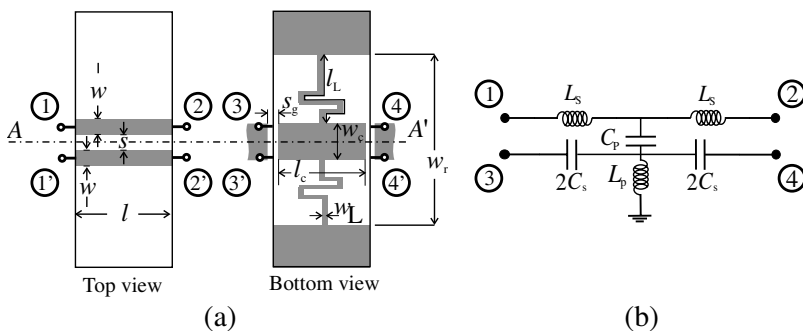


**Figure 2.** (a) Top and bottom views of a single unit cell of the proposed artificial transmission line (gray areas are the printed conductors). (b) Equivalent circuit for common-mode operation ( $AA'$  plane is a magnetic wall). The correspondence between physical and circuit model ports is indicated in the drawings.

## 2. ANALYSIS

In the double-side transmission line proposed for common-mode suppression in Fig. 1, a number (four in the figure) of identical rectangular patches connected to ground through narrow strips are etched in the ground plane side, below the pair of differential microstrip lines. A detail of the basic unit-cell of this structure is shown in Fig. 2(a). Note that the structure is symmetrical with respect to the  $AA'$  plane. In the frequency range of interest, the narrow meandered lines are intended to behave as quasi-lumped inductors. The pair of microstrip lines on the top side of the substrate are capacitively coupled to the patches.

### 2.1. Circuit Modeling of the Common Mode

Under common-mode excitation of the coupled strip lines (even mode using the terminology for single-ended circuits), the  $AA'$  plane is a magnetic wall and the current is then forced to flow partially through the  $LC$  resonators. This situation can be modeled by means of the equivalent circuit in Fig. 2(b) (common-mode operation). The circuit consists of two series inductances ( $L_s$ ) and a shunt to the ground  $LC$  series branch ( $L_p, C_p$ ). The capacitance  $C_p$  takes into account the capacitive coupling between the top and bottom metalization levels,  $L_p$  accounts for the inductance of the meandered lines, and  $L_s$  is the inductance of the top side printed strips. Two additional capacitors,  $C_s$ , have been included to account for the electric coupling between closely spaced rectangular patches (the separation gap is  $s_g$ ). If  $s_g$  is large enough,  $C_s$  can be neglected, thus obtaining a simple equivalent low-pass 2-port network. The structure would reject common-mode signals above the resonance frequency of the shunt connected  $LC$ -series branch. If the effect of  $C_s$  is not negligible, we should use a 4-port network description to analyze the influence of the DGS on common-mode operation. Either way, the structure provides strong rejection of the undesired common-mode noise over a relatively wide (in comparison to other reported solutions [12–14]) frequency band. Note that the equivalent circuit in Fig. 2(b) resembles the circuit proposed in [28] for the even mode, but the inductance  $L_p$  replaces here a resonant  $LC$  circuit in [28]. This resonant circuit makes the solution in [28] inherently narrower band.

Our proposed structure would be useful as a differential transmission system provided the differential (odd) propagating mode remains unaffected by the presence of the DGS pattern. Since the  $AA'$  plane behaves as a perfect electric conductor (odd mode), the return path for the odd mode current is only slightly affected by the

ground plane modifications. Indeed, current flowing through high impedance meandered lines is negligible because these inductors are short-circuited (physically or virtually) at their two ends. Most of the current flows through the straight coupled lines, with only a small portion flowing over the rectangular patches and through the gaps between them. Therefore, under differential mode operation, the structure will behave as an all-pass continuous transmission line with the characteristic impedance corresponding to the differential mode.

In order to verify the above qualitative reasoning, three prototypes have been fabricated on a substrate of thickness  $t = 0.49$  mm and  $\varepsilon_r = 2.43$ . The geometrical dimensions (see Fig. 2 for notation) are:  $w = 1.4$  mm,  $s = 2.4$  mm,  $l = 5.4$  mm,  $w_c = 5.2$  mm,  $l_c = 5$  mm,  $w_L = 0.2$  mm,  $l_L = 24.2$  mm,  $w_r = 14.6$  mm,  $s_g = 0.2$  mm. The values of some of these dimensions ( $w$ ,  $s$ ,  $w_c$ , and  $w_r$ ) have been obtained using the quasi-static algorithm in [29]. They have been adjusted to satisfy the  $50\ \Omega$  odd-mode characteristic impedance condition ( $100\ \Omega$  for the differential mode). This choice minimizes mismatching effects when the differential signal passes from the unpatterned to the patterned ground plane regions. Since that condition can be satisfied using various sets of dimensional parameters, the width,  $w$ , of the signal strips has been forced to be the one providing  $50\ \Omega$  characteristic impedance for the isolated microstrip line printed on the used substrate. Simulated (*Agilent ADS Momentum*) and measured common-mode insertion losses for three implementations (one, two, and four cascaded cells) of the proposed common-mode filtering section are shown in Fig. 3. The responses predicted by the equivalent circuit models (the circuit models are included in Fig. 3) have been represented for comparison purposes. The values of the circuit components have been extracted for the single unit cell. More specifically,  $C_p$  has been roughly approximated as the capacitance of a parallel plate capacitor of plate dimensions  $l \times w$  with the dielectric substrate between the plates;  $C_s$  has been approximated as the series gap capacitance of the equivalent  $\pi$ -circuit of a microstrip gap discontinuity between two strips of width  $w$  separated a distance  $s_g$  [30]; the value of  $L_p$  has been extracted from the location of the transmission zero close to 2 GHz. Note that the location of this zero can be tuned by controlling the length  $l_L$  of the meandered line inductor. Finally,  $L_s$  is chosen to fit the transmission level in the common-mode passband. The values of the lumped parameters for this case example are found to be:  $L_s = 4.20$  nH,  $C_p = 0.35$  pF,  $C_s = 0.022$  pF, and  $L_p = 16$  nH.

Due to the capacitive coupling between the inner conductor patches, the single transmission zero in Fig. 3(a) is split into two or three zeros when two or four unit cells are cascaded. Note that

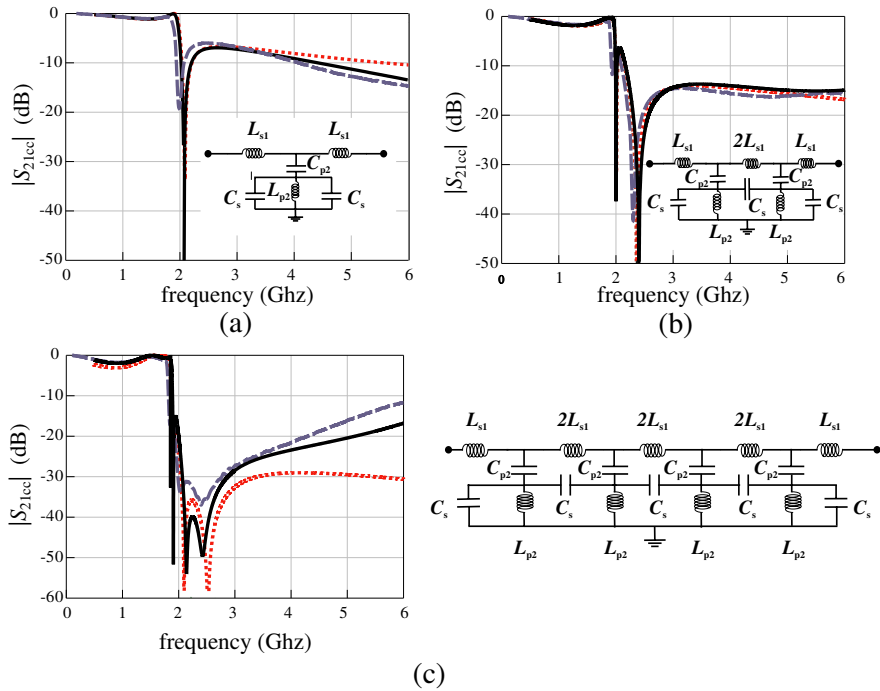


**Figure 3.** Full-wave simulated (solid black lines) and measured (blue dashed lines) common-mode responses for: (a) a single unit cell, (b) two cascaded unit cells, (c) four cascaded unit cells. Equivalent circuits and their predicted behavior (red dotted lines) are included.

$C_s$  approximately stands for the coupling to ground capacitors for the first and last patches. In the case of a single unit cell, the equivalent common-mode lumped circuit would strictly behave as a bandstop section rather than a low-pass section. However, the value of  $C_s$  is very small thus pushing the upper cutoff frequency pole towards a very high frequency value (18.5 GHz in the case treated in this example). Therefore, even taking into account the capacitors connected to ground, we can achieve a wide rejected frequency band. As expected, increasing the number of cells makes higher the rejection level of the common mode, at least in the range of frequencies for which the lumped equivalent circuit is reasonably valid. The insertion losses for the rejected band are above 6 dB for the single unit cell, 14 dB for the two unit-cells configuration, and 20 dB (2–4 GHz range) for the case with four unit cells. A reasonably good agreement can be found between measurements, EM simulations, and circuit simulations

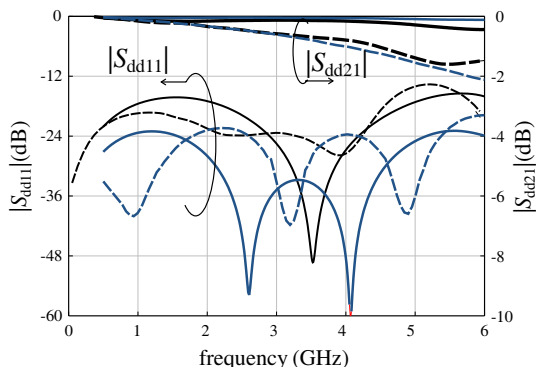


**Figure 4.** Measured (dashed lines) and calculated (solid lines) differential mode insertion ( $|S_{dd21}|$ ) and return ( $|S_{dd11}|$ ) losses of four cascaded cells of the proposed structure (black curves). The measured (dashed) and calculated (solid) response for a conventional pair of coupled lines (blue curves) has been included for comparison.

in Fig. 3. The results provided by the equivalent circuit seem to be less accurate at high frequencies as the number of cells is increased. Thus, although the use of four unit cells increases the rejection level at low frequencies, the high frequency behavior is deteriorated. The results in this paper are compared in Table 1 with other structures proposed in the literature. It can be seen that our proposal provides the largest fractional bandwidth while in a compact area.

**Table 1.** Comparison of several differential lines providing common mode suppression.

Ref.	Length ( $\lambda_e$ )	Width ( $\lambda_e$ )	Area ( $\lambda_e^2$ )	FBW (%) -20 dB
[12]	0.76	0.47	0.36	50
[13]	0.44	0.44	0.19	—
[14]	0.64	0.13	0.08	41
[28]	0.26	0.16	0.04	32
This	0.32	0.22	0.07	67

In Fig. 4 we show the measured and simulated differential mode transmission for the four cells structure in Fig. 3 and for a simple pair of differential microstrip lines without ground plane etching. From

the measured data in Fig. 4 we can conclude that the presence of the patches and meandered lines in the ground plane side of the substrate does not meaningfully affect the differential mode operation, as expected and desired. Note that transmission degrades at relatively high frequencies in both cases (patterned and unpatterned ground planes). This is due to differential-to-common mode conversion associated to unavoidable unbalanced loading in our measurement setup. This degradation is not observed in the full-wave simulations since in such case symmetries are perfect.

## 2.2. Bloch-Floquet Analysis

The common-mode rejection behavior can be explained in terms of the dispersion equation for the Bloch waves supported by a periodic structure consisting of the cascade connection of an infinite number of identical unit cells (as the one depicted in Fig. 2(a)). This Bloch-Floquet analysis has been carried out, for instance, in [14, 28] to explain the stopband common-mode operation of the proposed structures in terms of the forbidden band of the periodic structures. In order to apply a similar analysis to the structure proposed in Fig. 1, we first carry out a simplified study where it is neglected the coupling capacitor between ground plane patches. If  $C_s = 0$ , the circuit in Fig. 2(b) becomes a simple 2-port network whose dispersion relation can be obtained from the  $ABCD$  transmission matrix of the unit cell [31, Chap. 8] as

$$\cosh(\gamma l) = A. \quad (1)$$

In the above equation,  $\gamma$  is the complex propagation constant of the Bloch wave ( $\gamma = \alpha + j\beta$ ),  $l$  is the length of the unit cell, and the element  $A$  of the transmission matrix is given by

$$A = \frac{1 - \omega^2 C_p (L_p + L_s)}{1 - \omega^2 L_p C_p} \quad (2)$$

where  $\omega$  is the angular frequency. For the previously extracted values of the circuit parameters, (1) and (2) yield  $\beta = 0$  and  $\alpha \neq 0$  (no propagation, only attenuation) from 2.1 GHz onwards; namely, there is not an alternating sequence of allowed/forbidden bands as in [14, 28]. The structure behaves as a low-pass filter rather than as a bandstop filter. However, it should be mentioned that the distributed effects not included in this simplified circuit model will modify this prediction at frequencies above the range of interest of this paper. Nevertheless, the low-pass filtering behavior here obtained qualitatively explains why our proposed structure provides good common-mode rejection over a wide frequency band.

Unfortunately, to ignore the nonvanishing value of  $C_s$  might be not very realistic. Actually, closely spaced patches in the bottom side of the substrate are desirable since they would provide a better differential mode performance. If the interaction between adjacent patches is accounted for by a non-negligible edge coupling capacitance ( $C_s \neq 0$ ), the resulting equivalent-circuit unit cell should be treated as a 4-port network, as suggested in [14, 32] for other structures. Starting from a 4-port  $ABCD$  matrix formulation, following the guidelines in [14, 32], the dispersion equation can be written as follows:

$$\det\{[\mathbf{A}] - \cosh(\gamma l)[\mathbf{I}]\} = 0 \tag{3}$$

where  $[\mathbf{I}]$  is the unit matrix and  $[\mathbf{A}]$  the  $2 \times 2$  matrix that relates the voltages of the left (input) side of the 4-port network in Fig. 2(b) [ $V_1$  and  $V_3$ ] to the voltages of the right (output) side [ $V_2$  and  $V_4$ ] provided the right side ports are open circuited; namely,

$$\begin{bmatrix} V_1 \\ V_3 \end{bmatrix} = \begin{bmatrix} A_{11} & A_{12} \\ A_{21} & A_{22} \end{bmatrix} \begin{bmatrix} V_2 \\ V_4 \end{bmatrix} \quad \text{for } I_2 = I_4 = 0. \tag{4}$$

For the 4-port network in Fig. 2(b), the elements of the matrix  $[\mathbf{A}]$  are readily found to be

$$A_{11} = 1 - \omega^2 L_s C_p \tag{5}$$

$$A_{12} = \omega^2 L_s C_p \tag{6}$$

$$A_{21} = -\frac{C_p}{2C_s} \tag{7}$$

$$A_{22} = 1 + \frac{C_p}{2C_s} - \frac{1}{\omega^2 L_p C_s}. \tag{8}$$

The solution of Eq. (3) leads to the two following modal solutions for  $\gamma$ :

$$\cosh(\gamma l) = \frac{1}{2} \left( A_{11} + A_{22} \pm \sqrt{(A_{11} - A_{22})^2 + 4A_{12}A_{21}} \right). \tag{9}$$

It should be noted that the two solutions come from the  $\pm$  choice in (9) and that, if  $\gamma$  is a solution of (9),  $-\gamma$  will also be another solution.

In Fig. 5 we have plotted the behavior of the positive real and imaginary parts of the two modal propagation constants. In the low-frequency region up to  $\sim 1.8$  GHz, one mode is propagative (blue-color solution with  $\alpha = 0, \beta \neq 0$ ) and the other is evanescent (red-color solution with  $\alpha \neq 0, \beta = 0$ ). Above 3.0 GHz, the two modes are purely evanescent ( $\alpha \neq 0, \beta = 0$ ) and then they do not carry active power. In the middle interval (1.8–3.0 GHz), the 4-port equivalent circuit predicts the existence of complex modes ( $\alpha \neq 0, \beta \neq 0$ ). Since complex modes are excited by a single source in pairs and each pair

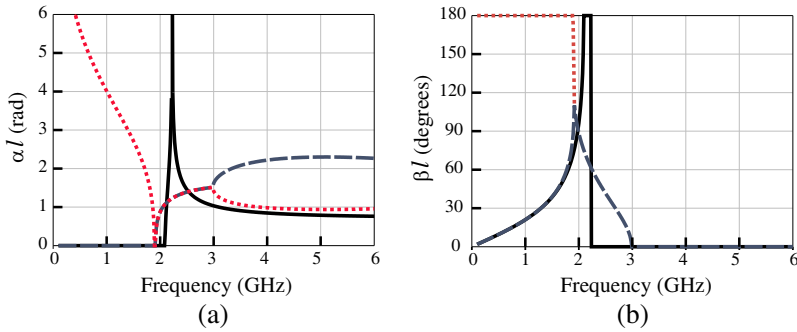


**Figure 5.** Real (a) and imaginary (b) parts of the two propagation constants of the Bloch waves that exist in a periodic structure whose unit cell is the 4-port network shown in Fig. 2(b). The dispersion curves obtained with the 2-port model are also included for comparison purposes (solid black lines).

of complex modes do not carry active power (see [33] and references therein), all the frequencies above 1.8 GHz can be considered as part of a forbidden region. Thus, the prediction of the 4-port model sustains the qualitative prediction of the simpler 2-port one in the sense of showing a low-pass filter behavior for the infinite periodic structure. The existence of complex modes predicted by 4-port model slightly pushes down the cutoff frequency of the low-pass filter when compared with the prediction of the 2-port model, and it is now closer to the observed simulated and measured transmission coefficients reported in Fig. 3(c) for the implemented 4-cells common-mode filter. Since allowed and rejected bands of the periodic structure are linked to the values of the lumped components that define the unit cell, the Bloch-Floquet analysis of the periodic structure also gives us an interesting physical insight on the relevant parameters that control the onset frequency of the rejected band as well as the attenuation of the supported non-propagating (evanescent or complex) modes.

### 3. EYE DIAGRAM

The structure that has been proposed to cancel out the common-mode signal should be as transparent as possible for the differential signal. Thus, we now demonstrate that this structure preserves a good differential signal quality. This is done by comparing the measured eye diagrams for a conventional pair of coupled strips and for the defected ground structures studied in this paper (without unperturbed ground

	Reference structure	Proposed Structure
Eye Height	377 mV	375 mV
Eye width	397 ps	396 ps
Jitter	2.66 ps	4.33 ps

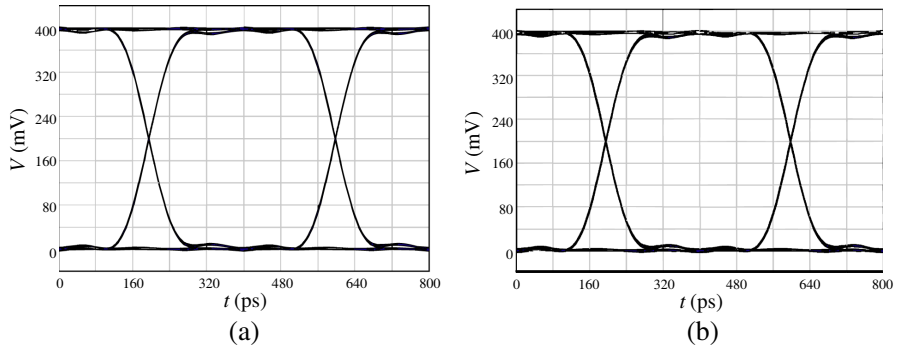


**Figure 6.** Measured differential eye diagrams for (a) a conventional pair of coupled lines (without etching in the ground plane) and (b) for the structure proposed in this paper.

plane, no common-mode rejection is provided but differential mode performance should be optimum). The measured eye diagrams for a 2.5 Gb/s, 200 mV differential-mode excitation are plotted in Fig. 6. The two compared structures have the same length. The eye diagram is used to evaluate the signal integrity of the channel in terms of eye width, eye height, and jitter. We have found that the quality of the eye diagram for the proposed common-mode rejection filter is barely distinguished from that of the reference structure. The eye diagram parameters have been summarized at the top of Fig. 6. The eye height and the eye width are 377 mV and 397 ps respectively for the reference structure, and 375 mV and 396 ps for the proposed differential lines. Thus, no degradation is observed in these parameters. The jitter variation (2.66 ps in the reference structure and 4.43 ps in the newly proposed structure) is not very relevant considering that the bit period is 400 ps.

#### 4. BALANCED DUAL-BAND BANDPASS FILTER

Once the weak influence of the DGS structure on the differential mode propagation has been verified, we will illustrate in this section its use to improve the common-mode performance of a non-optimized balanced dual-band filter. The design is based on the introduction

of only a couple of cells of the structure in Fig. 2 as input/output stages of the dual-band balanced filter. This procedure allows for the design of differential filters by simply using standard techniques for the differential response without paying attention to the common-mode behavior. Then, there is no need to develop specific simultaneous solutions for both common-mode suppression and differential-mode specs [1–3, 5]. This technique has been successfully applied to design single-band bandpass filters [14, 15], for which a relatively narrowband common-mode rejection device is sufficient. For dual-band applications a wide operation band is necessary. In this paper we exploit the relative wideband behavior of the proposed common-mode rejection structure to design a balanced dual-band bandpass filter, such as the ones reported in [5, 34, 35]. The basic dual-band filter used in our implementation is based on the single-ended dual-band filter reported in [27]. The straightforward conversion of the single-ended filter in [27] to its balanced version has very poor common-mode rejection. However, the combination of the dual-band design with our common-mode rejection structure leads to a good overall performance.

The proposed layout, including the common-mode rejection stages, is shown in Fig. 7(a). Basically the filter consists of the combination in the same structure of two subfilters working at two different frequencies and whose specs can be almost independently tuned (see Fig. 7). The two passbands are centered at the resonance

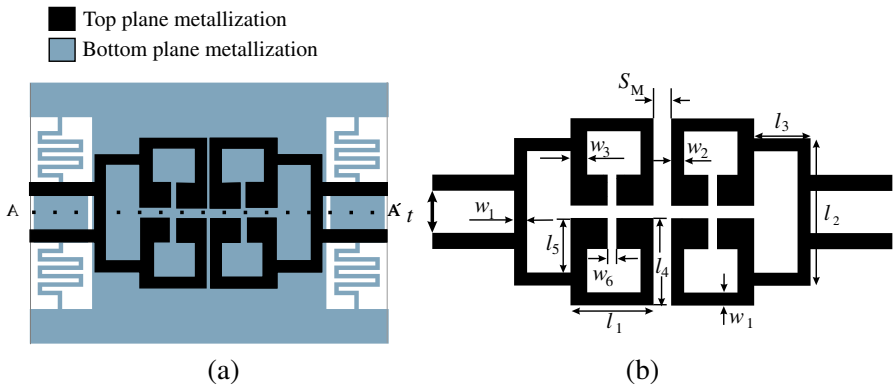


**Figure 7.** (a) Layout of the proposed dual-band filter with the common-mode suppression stages. (b) Final dimensions of the resonators:  $s = 1$  mm,  $s_M = 0.2$  mm,  $t = 3.2$  mm,  $w_1 = 0.3$  mm,  $w_2 = 0.3$  mm,  $w_3 = 0.6$  mm,  $w_4 = 2$  mm,  $w_5 = 2.5$  mm,  $w_6 = 0.2$  mm,  $l_1 = 4.2$  mm,  $l_2 = 10.4$  mm,  $l_3 = 1.3$  mm,  $l_4 = 5.3$  mm.

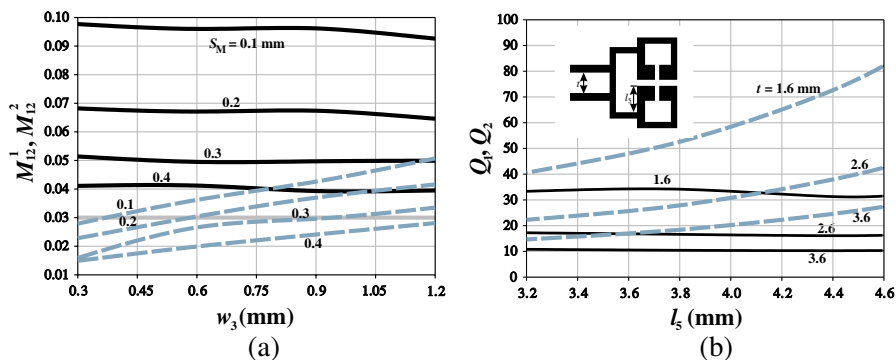


**Figure 8.** (a) Coupling coefficients for the first ( $M_{1,2}^{(1)}$ : solid lines) and second ( $M_{1,2}^{(2)}$ : dashed lines) bands as a function of the ratio  $w_3/w_2$  using  $s_M$  as parameter. (b) External quality factor at the first ( $Q_1$ : solid lines) and second ( $Q_2$ : dashed lines) resonance frequencies versus  $l_5$  using  $t$  as parameter. The other geometrical dimensions have the values show in Fig. 7.

frequencies of the large ( $f_{c1}$ ) and small ( $f_{c2}$ ) folded resonators that can be identified in Fig. 7. This filter use the same working principles that the one in [27] but, in order to provide balanced operation, four symmetrically located access ports have been used. A relevant advantage of this filter is the possibility of independent control of the specs (fractional bandwidth, ripple) of each band under differential-mode operation. As is well known [36], the coupling coefficients between adjacent resonators and the external quality factors of the input/output resonators are the design parameters to be adjusted in order to achieve the filter specs. In Fig. 8(a) we show the simulated coupling coefficients for the two bands of the filter as a function of the width  $w_3$  (see Fig. 7) using  $s_M$  as parameter. The remaining geometrical parameters have the values shown in the caption of Fig. 7. They have been calculated to get  $f_{c1} = 2.5$  GHz and  $f_{c2} = 5.3$  GHz. Note that, for the first band, the coupling coefficient  $M_{1,2}^{(1)}$  mainly depends on  $s_M$  (distance between resonators). This distance is the used to achieve the required value of  $M_{1,2}^{(1)}$ . Once the value of  $s_M$  is fixed,  $w_3$  is adjusted to obtain the coupling coefficient,  $M_{1,2}^{(2)}$ , corresponding to the second band specs (note that  $f_{c1}$  and  $f_{c2}$  barely change in the considered range). Following a similar reasoning, we have plotted in Fig. 8(b) the external quality factor at  $f_{c1}$  and  $f_{c2}$  as a function of  $l_5$  using the separation  $t$  between the input/output lines as a parameter.

The distance  $t$  determines the quality factor of the first band,  $Q_1$ , which is almost independent of the connection point to the small resonator ( $l_5$ ). Therefore, once  $t$  has been fixed to determine  $Q_1$ , we are free of tuning  $l_5$  to reach the required value of the external coupling factor for the second band,  $Q_2$ .

As an example, we report the design of a dual-band Butterworth filter (order  $N = 2$ ) with central frequencies  $f_{c1} = 2.5$  GHz and  $f_{c2} = 5.3$  GHz and fractional bandwidths  $\text{FBW}_1 = 10\%$  and  $\text{FBW}_2 = 4\%$ . From these specs, the required coupling coefficients and external quality factors are:  $M_{1,2}^{(1)} = 0.071$ ,  $M_{1,2}^{(2)} = 0.028$ ,  $Q_1 = 14.2$ , and  $Q_2 = 35.4$ . The final dimensions of the filter are detailed in the caption of Fig. 7. It is important to note that the I/O coupled differential lines have to be designed to provide good common-mode rejection within the differential filter passbands. Thanks to the wideband behavior of the I/O common-mode filtering sections, it is expected that common-mode propagation is rejected within the two passbands, while the differential-mode response is not meaningfully degraded by the presence of the

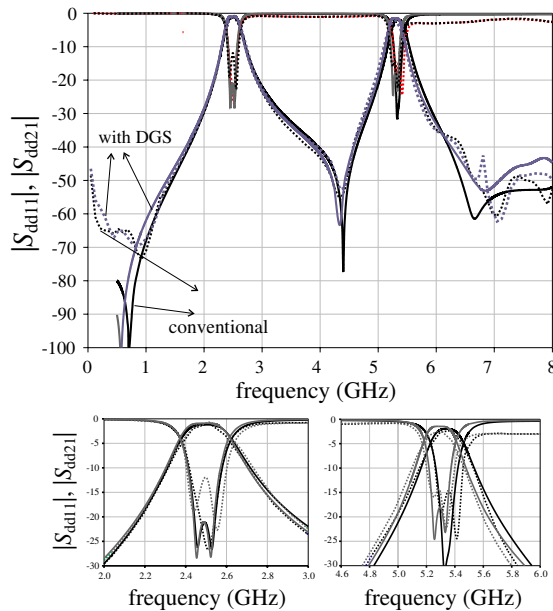


**Figure 9.** Differential-mode response of the proposed dual-band filter. [Solid lines]: simulation results, [dotted lines]: measurements. Black curves are for the filter without common-mode suppression section.

ground plane etching.

Fig. 9 shows the simulated and measured differential-mode responses of the balanced filter with (modified) and without (conventional) the common-mode rejection I/O stages. The measured center frequencies, 3-dB fractional bandwidths, and insertion losses of the two passbands are summarized in Table 2 for both, the conventional and the modified filter implementations. These values clearly illustrate that the introduction of the common-mode rejection sections does not appreciably affect the differential mode performance. However, common-mode noise is strongly rejected in the two passbands of the dual-band modified filter, in contrast with the poor behavior of the conventional version. This can be clearly appreciated in Fig. 10, where only the common-mode response is plotted. In the first transmission band the improvement of common-mode rejection attributable to the added I/O sections is around 22 dB, and around 17 dB for the upper transmission band.

**Table 2.** Measured filter specs.

	First passband			Second passband		
	$f_{c1}$ (GHz)	FBW <sub>1</sub> (%)	IL <sub>1</sub> (dB)	$f_{c2}$ (GHz)	FBW <sub>2</sub> (%)	IL <sub>2</sub> (dB)
Conv.	2.50	9.6	1.38	5.35	4.01	2.10
Modif.	2.50	11	1.46	5.27	3.98	2.22

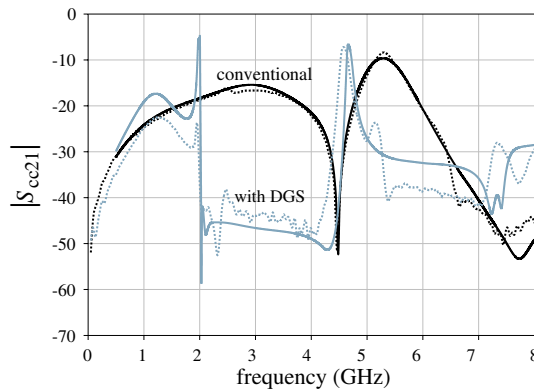


**Figure 10.** Common-mode insertion losses of the proposed filter. [Solid lines]: simulation results, [dotted lines]: measurements. Black curves are for the filter without common-mode suppression sections.

## 5. CONCLUSIONS

In this work, an approach for the design of differential lines with common-mode suppression in the gigahertz frequency range has been presented. The differential transmission lines have been implemented using double-side microstrip technology. The structure exhibits all-pass behavior under differential-mode operation and broadband rejection under common-mode operation. Thanks to this broadband operation, the structure can be combined with dual-band balanced filters to drastically improve their common-mode features. Thus, the use of a couple of unit cells as input/output stages can provide 15–25 dB common-mode rejection level improvement in the two bands even if they are very separated. A new dual-band balanced filter inspired in a previously reported single-ended dual-band filter has been introduced to illustrate the application of the method.

## ACKNOWLEDGMENT

This work has been funded by the Spanish Ministerio de Ciencia e Innovación with European Union FEDER funds (project No. TEC2010-16948 and CSD2008-00066) and by the Spanish Junta de Andalucía (TIC-112).

## REFERENCES

1. Wu, C.-H., C.-H. Wang, and C. H. Chen, “Novel balanced coupled-line bandpass filters with common-mode noise suppression,” *IEEE Trans. Microw. Theory Tech.*, Vol. 55. No. 2, 287–295, Feb. 2007.
2. Wu, C.-H., C.-H. Wang, and C. H. Chen, “Balanced coupled-resonator bandpass filters using multisection resonators for common-mode suppression and stopband extension,” *IEEE Microw. Wireless Compon. Lett.*, Vol. 17. No. 7, 507–509, Jul. 2007.
3. Wu, C.-H., C.-H. Wang, and C. H. Chen, “Stopband-extended balanced bandpass filter using coupled stepped-impedance resonators,” *IEEE Trans. Microw. Theory Tech.*, Vol. 55. No. 8, 1756–1763, Aug. 2007.
4. Wang, X.-H., Q. Xue, and W.-W. Choi, “A novel ultra-wideband differential filter based on double-sided parallel-strip line,” *IEEE Microw. Wireless Compon. Lett.*, Vol. 20, No. 8, 471–473, Aug. 2010.
5. Shi, J. and Q. Xue, “Novel balanced dual-band bandpass filter

- using coupled stepped impedance resonators,” *IEEE Microw. Wireless Compon. Lett.*, Vol. 20, No. 1, 19–21, Jan. 2010.
6. Wu, S.-M., C.-T. Kuo, and C.-H. Chen, “Very compact full differential bandpass filter with transformer integrated using integrated passive device technology,” *Progress In Electromagnetic Research*, Vol. 113, 251–267, 2011.
  7. Wu, S. M., C.-T. Kuo, P.-Y. Lyu, Y.-L. Shen, and C.-I. Chien, “Miniaturization design of full differential bandpass filter with coupled resonators using embedded passive device technology,” *Progress In Electromagnetic Research*, Vol. 121, 365–379, 2011.
  8. Lin, S.-C. and C.-Y. Yeh, “Stopband-extended balanced filters using both  $\lambda/4$  and  $\lambda/2$  SIRS with common-mode suppression and improved passband selectivity,” *Progress In Electromagnetic Research*, Vol. 128, 215–228, 2012.
  9. Yanagisawa, K., F. Zhang, T. Sato, K. Yamasawa, and Y. Miura, “A new wideband common-mode noise filter consisting of Mn-Zn ferrite core and copper/polyimide tape wound coil,” *IEEE Trans. Magn.*, Vol. 41, No. 10, 3571–3573, Oct. 2005.
  10. Deng, J. and K. Y. See, “In-circuit characterization of common-mode chokes,” *IEEE Trans. Electromagn. Compat.*, Vol. 49, No. 2, 451–454, May 2007.
  11. Tseng, B.-C. and L.-K. Wu, “Design of miniaturized common-mode filter by multilayer low-temperature co-fired ceramic,” *IEEE Trans. Electromagn. Compat.*, Vol. 46, No. 4, 471–579, Nov. 2004.
  12. Liu, W.-T., C.-H. Tsai, T.-W. Han, and T.-L. Wu, “An embedded common-mode suppression filter for GHz differential signals using periodic defected ground plane,” *IEEE Microw. Wireless Compon. Lett.*, Vol. 18, No. 4, 248–250, Apr. 2008.
  13. Wu, S.-J., C.-H. Tsai, T.-L. Wu, and T. Itoh, “A novel wideband common-mode suppression filter for gigahertz differential signals using coupled patterned ground structure,” *IEEE Trans. Microw. Theory Tech.*, Vol. 57, No. 4, 848–855, Apr. 2009.
  14. Naqui, J., A. Fernández-Prieto, M. Durán-Sindreu, F. Mesa, J. Martel, F. Medina, and F. Martín, “Common mode suppression in microstrip differential lines by means of complementary split ring resonators: Theory and applications,” *IEEE Trans. Microw. Theory Tech.*, Vol. 60, No. 10, 3023–3034, Oct. 2012.
  15. Fernández-Prieto, A., J. Martel, J. S. Hong, F. Medina, S. Qian, and F. Mesa, “Differential transmission line for common-mode suppression using double side MIC technology,” *Proc. of the 41st European Microwave Conference (EuMC)*, 631–634, Manchester,

- England, UK, Oct. 10–13, 2011.
16. Ma, D.-C., Z.-Y. Xiao, L.-L. Xiang, X.-H. Wu, C.-Y. Huang, and X. Kou, “Compact dual-band bandpass filter using folded SIR with two stubs,” *Progress In Electromagnetics Research*, Vol. 117, 357–364, 2011.
  17. Kuo, J.-T., C.-Y. Fan, and S.-C. Tang, “Dual-wideband bandpass filters with extended stopband on coupled-line and coupled three-line resonators,” *Progress In Electromagnetic Research*, Vol. 124, 1–15, 2012.
  18. Chaudhary, G., Y. Jeong, K. Kim, and D. Ahn, “Design of dual-band bandpass filters with controllable bandwidths using new mapping function,” *Progress In Electromagnetic Research*, Vol. 124, 17–34, 2012.
  19. Wang, M., X. Li, and H. Wang, “Dual-band and harmonic suppression of filter designs based on asymmetric half-wavelength resonator,” *Journal of Electromagnetic Waves and Applications*, Vol. 26, No. 16, 2192–2201, 2012.
  20. Wang, J., H. Ning, Q. Xiong, M. Li, and L. Mao, “A novel miniaturized dual-band bandstop filter using dual-plane defected structures,” *Progress In Electromagnetic Research*, Vol. 134, 397–417, 2013.
  21. Karpuz, C., A. K. Gorur, A. N. Basmaci, and A. Ozek, “Design and analysis of a compact dual-mode dual-band microstrip bandpass filter,” *Journal of Electromagnetic Waves and Applications*, Vol. 27, No. 2, 180–190, 2013.
  22. Zhang, L.-Z., L. Zhou, and W. Jiang, “A compact dual-band coupler with arbitrary power dividing ratio using broadside-coupled microstrip,” *Journal of Electromagnetic Waves and Applications*, Vol. 27, No. 2, 140–148, 2013.
  23. Yang, C.-F., Y.-C. Chen, C.-Y. Kung, J.-J. Lin, and T.-P. Sun, “Design and fabrication of a compact quad-band bandpass filter using two different parallel positioned resonators,” *Progress In Electromagnetics Research*, Vol. 115, 159–172, 2011.
  24. Chen, W.-Y., M.-H. Weng, S.-J. Chang, H. Kuan, and Y.-H. Su, “A new tri-band bandpass filter for GSM, Wimax and ultra-wideband responses by using asymmetric stepped impedance resonators,” *Progress In Electromagnetic Research*, Vol. 124, 365–381, 2012.
  25. Li, C.-Y., J.-X. Chen, H. Tang, L.-H. Zhou, J. Shi, and Z.-H. Bao, “Tri-band bandpass filter with wide stop-band using stub-loaded triple-mode resonator,” *Journal of Electromagnetic Waves and Applications*, Vol. 27, 439–447, 2013.

26. Lee, C.-H, C.-I. G. Hsu, H.-H. Chen, and Y.-S. Lin, "Balanced single- and dual-band BPFs using ring resonators," *Progress In Electromagnetic Research*, Vol. 116, 333–346, 2011.
27. Chen, C.-Y., C.-Y. Hsu, and H.-R. Chuang, "Design of miniature planar dual-band filter using dual-feeding structures and embedded resonators," *IEEE Microw. Wireless Compon. Lett.*, Vol. 16, No. 12, 669–671, Dec. 2006.
28. Tsai, C.-H. and T.-L. Wu, "A broadband and miniaturized common-mode filter for gigahertz differential signals based on negative-permittivity metamaterials," *IEEE Trans. Microw. Theory Tech.*, Vol. 58, No. 1, 195–202, Jan. 2010.
29. Martel, J. and F. Medina, "A suitable integral equation for the quasi-TEM analysis of hybrid strip/slot-like structures," *IEEE Trans. Microw. Theory Tech.*, Vol. 49, No. 1, 224–227, Jan. 2001.
30. Martel, J., R. R. Boix, and M. Horno, "Static analysis of microstrip discontinuities using the excess charge density in the spectral domain," *IEEE Trans. on Microwave Theory Tech.*, Vol. 39, No. 9, 1623–1631, Sep. 1991.
31. Pozar, D. M., *Microwave Engineering*, 3rd Edition, Wiley & Sons, 2005.
32. Islam, R., M. Zedler, and G. V. Eleftheriades, "Modal analysis and wave propagation in finite 2D transmission-line metamaterials," *IEEE Trans. Microw. Theory Tech.*, Vol. 59, 1562–1570, May 2011.
33. Freire, M. J., F. Mesa, and M. Horno, "Excitation of complex and backward modes on shielded lossless printed lines," *IEEE Trans. Microw. Theory Tech.*, Vol. 47, 1098–1105, Jul. 1999.
34. Shi, X. and Q. Xue, "Balanced bandpass filters using center-loaded half-wavelength resonators," *IEEE Trans. Microw. Theory Tech.*, Vol. 58, No. 4, 970–977, Apr. 2010.
35. Shi, X. and Q. Xue, "Dual-band and wide-stopband single-band balanced bandpass filters with high selectivity and common-mode suppression," *IEEE Trans. Microw. Theory Tech.*, Vol. 58, No. 8, 2204–2212, Aug. 2010.
36. Hong, J.-S., *Microstrip Filters for RF/Microwave Applications*, 2nd Edition, Wiley, New York, 2011.